RESEARCH ARTICLE

FASEB BioAdvances WILEY

Ogerin induced activation of Gpr68 alters tendon healing

Andrew Rodenhouse[1] | Gilbert Smolyak[1] | Emmanuela Adjei-Sowah[1] | Neeta Adhikari[1] | Samantha Muscat[1] | Takuma Okutani[2] | Constantinos Ketonis[1] | Anne E. C. Nichols[1] | Robert M. Kottmann[2] | Alayna E. Loiselle[1]

[1]Center for Musculoskeletal Research, Department of Orthopaedics & Physical Performance, University of Rochester Medical Center, Rochester, New York, USA

[2]Department of Medicine, University of Rochester Medical Center, Rochester, New York, USA

Correspondence
Alayna E. Loiselle, Center for Musculoskeletal Research, Department of Orthopaedics & Physical Performance, University of Rochester Medical Center, 601 Elmwood Ave, Box 665-G, Rochester, NY 14642, USA.
Email: alayna_loiselle@urmc.rochester.edu

Abstract

Satisfactory outcomes after acute tendon injuries are hampered by a fibrotic healing response. As such, modulation of extracellular matrix deposition and re-modeling represents an important intervention point to improve healing. During fibrosis, matrix is deposited and remodeled by activated fibroblasts and/or myofibroblasts. Recent work has demonstrated that Ogerin, a positive allosteric modulator of the orphan proton-sensing GPCR, GPR68, can modulate fibroblast ↔ myofibroblast dynamics in multiple fibroblast populations, including blunting myofibroblast differentiation and facilitating reversion of mature myofibroblasts to a basal fibroblast state in vitro. In the present study, we tested the ability of Ogerin to modulate tendon fibroblast ↔ myofibroblast behavior in vitro and in vivo. Consistent with prior work, Ogerin can both blunt TGF-β induced teno-cyte → myofibroblast differentiation and partially revert mature myofibroblasts to a basal tenocyte state. However, Ogerin treatment from days 8–12 after tendon repair surgery did not inhibit myofibroblast differentiation, and Ogerin treatment from post-operative days 24–28 did not induce myofibroblast reversion. Moreover, while we expected Ogerin treatment from days 8–12 to impair heal-ing due to blunted extracellular matrix formation, Ogerin treatment improved tendon mechanical properties and altered cell transcriptional profiles and com-munication patterns in a way that suggests accelerated remodeling and resolu-tion of the repair response, identifying Ogerin as a novel therapeutic approach to improve the tendon healing process.

KEYWORDS
fibrosis, Gpr68, myofibroblasts, Ogerin, tendon healing

1 | INTRODUCTION

Due to their superficial anatomic locations, traumatic injuries to tendons are very common. For example, flexor tendon injuries have an estimated incidence of 4.8 per 100,000 persons and remain arguably one of the most challenging injuries facing hand surgeons.[1] Moreover, tendon injuries pose a significant economic burden to the United States' health care system, costing between $240.8 and $409.1 million annually.[2] Following surgical repair of tendon injuries, patient outcomes are unpredictable, and complication rates remain high despite modern surgical and rehabilitation techniques.[3–6] Importantly, there are no current therapeutic strategies to mitigate these complications, emphasizing the pressing need for the development of therapeutics to improve tendon healing outcomes.

While the overall molecular regulators of fibrotic tendon healing are incompletely defined, activated fibroblasts/myofibroblasts are key regulators of both physiologic and pathologic aspects of healing. Myofibroblasts produce, remodel, and contract the extracellular matrix[7–11] during the proliferative phase of healing. However, failure to undergo apoptosis or revert to a basal-like state allows for prolonged, persistent myofibroblast activity, with extracellular matrix (ECM) deposition outpacing tissue remodeling, resulting in tissue fibrosis and peritendinous adhesion formation. As such, pharmacological approaches to modulate myofibroblasts hold great potential as a means to promote tissue regeneration and prevent tissue fibrosis.[7–11] Recently, Ogerin has been identified as a positive allosteric modulator of the proton-sensing G-protein coupled receptor GPR68/OGR1[12,13] that can modulate fibroblast ↔ myofibroblast dynamics in multiple fibroblast populations including lung, dermis, and intestine.[14] More specifically, Ogerin treatment blunts TGF-β induced fibroblast → myofibroblast differentiation, and Ogerin treatment following myofibroblast differentiation promotes reversion to a basal fibroblast state.[14] This ability to modulate both myofibroblast differentiation and reversion highlights the translational potential of Ogerin to enhance tendon healing when delivered during different phases of healing. Therefore, in the present study, we tested the ability of Ogerin to mediate tendon fibroblast ↔ myofibroblast dynamics in vitro and during in vivo tendon healing in a murine model. Ogerin was delivered during the proliferative phase of healing (post-operative days [POD] 8–12), and we hypothesized that Ogerin-mediated inhibition of myofibroblast differentiation would impair healing due to decreased extracellular matrix formation and remodeling. Moreover, an additional arm of the study tested the hypothesis that Ogerin treatment during the remodeling phase (POD 24–28) would promote myofibroblast reversion.

2 | MATERIALS AND METHODS

2.1 | Primary tendon cell isolation and in vitro studies

Tendon cells were isolated as previously described.[15] Briefly, for each experiment, 4–6 flexor digitorum longus (FDL) tendons were aseptically harvested from 10- to 12-week-old female C57Bl/6J mice (#000664, Jackson Laboratory, Bar Harbor, ME), pooled together, and digested in Fibroblast Growth Medium-2 (FGM-2; #CC-3132, Lonza, Basel, Switzerland) containing collagenase (0.075% collagenase I; #C6885, Sigma). Cells were plated on collagen-coated (rat tail collagen type 1, $5\,\mu g/cm^2$; #354236, Corning, Tewksbury, MA) plates under standard culture conditions. After 5–7 days in culture (passage 0), cells were passaged at 70% confluence (~3–5 days after plating) and all experiments were conducted with cells at passage 1 or 2. In the first experiment (inhibition of myofibroblast differentiation), cells were treated with 1 ng/mL TGF-β (R&D Systems) to induce myofibroblast differentiation,[15] and/or Ogerin (50–150 μM) (#5722, Tocris, Minneapolis, MN), and/or vehicle control (60:40 DMSO: Saline) for 24 h. In the second experiment (myofibroblast reversion), cells were treated with 1 ng/mL TGF-β or vehicle for 24 h to induce myofibroblast differentiation. After 24 h, media containing TGF-β was removed, and cells were washed 2x with PBS. Cells were then treated with 150 μM Ogerin or vehicle for an additional 48 h. Cells were fixed, permeabilized, and stained with α-SMA-Cy3 (1:200, C6198, Sigma Life Sciences) and NucBlue™ Live ReadyProbes™ Reagent (Hoechst 33342) (#R37605, ThermoFisher). Slides were imaged with the VS120 Virtual Slide Microscope (Olympus, Waltham, MA, USA) and processed with Olyvia software (Olympus, Waltham MA, USA). Three random imaging fields per well were used for point counting of fully differentiated myofibroblasts (αSMA+ stress fibers) and quantification was done in ImageJ. All experiments were performed in biological triplicates.

2.2 | In vivo studies

All animal studies were reviewed and approved by the University Committee on Animal Research (UCAR) at the University of Rochester Medical Center (UCAR Number: 2014-004E). The study was carried out in strict accordance with the Guide for Care and Use of Laboratory Animals.

2.3 | Murine model of flexor tendon repair

At 10–12 weeks of age, female C57BL/6J mice underwent transection and repair of the FDL tendon of the right hind-paw as previously described using standard micro-surgical technique.[16] Briefly, mice were anesthetized with intraperitoneal ketamine (50–75 mg/kg)/dexmedetomidine (0.5–1 mg/kg), before administration of subcutaneous Buprenorphine ER (0.5–1.0 mg/kg). After sterilization of the surgical site, an incision was made in the calf, and the FDL was identified and sharply transected at the myotendinous junction to prevent early rupture of the repair site, before the skin was closed with 5–0 nylon suture. Thereafter, a separate incision was made on the plantar hind-paw. The FDL tendon was again isolated and transected just proximal to its bifurcation before being repaired with 8–0 nylon suture. The skin was then closed with 5–0 nylon suture. Following FDL repair surgery, mice were treated with either Ogerin (20 mg/kg) or vehicle (60:40 DMSO: sterile saline) via once daily IP injections during the designated treatment window: Experiment #1: post-operative day (POD) 8–12 to blunt myofibroblast differentiation; or Experiment #2: POD 24–28 to promote myofibroblast reversion.

2.4 | Histology and immunofluorescence

Mice were sacrificed at either POD 14 (Experiment #1) or POD 28 (Experiment #2) ($n = 5$–6 per treatment group per timepoint). Hind-paws were harvested, fixed in 10% neutral buffer formalin (72 h), decalcified in Webb-Jee EDTA solution (14 days), processed, and embedded in paraffin. Three-micron sections were cut through the sagittal plane of the hind-paw, and de-waxed, rehydrated sections underwent staining to define tissue morphology using Alcian Blue/Hematoxylin/Orange G (ABHOG), collagen ECM using Masson's Trichrome, or immunofluorescent analysis. For immunofluorescence, sections were probed with antibodies against phosphorylated-CREB (Ser133) (1:100, #9198, Cell Signaling Technology, Danvers, MA), αSMA-Cy3 (1:250, #C6198, Sigma-Aldrich, St. Louis, MO), F4/80-AlexaFluor647 (1:100, #Ab307470, Abcam), and Ly6G (1:100, #RB6-8C5, Novus USA, Centennial, CO). For phosphorylated-CREB, a FITC-conjugated Donkey anti-rabbit secondary antibody was used (1: 200, #711–095-152, Jackson Immuno, West Grove, PA, USA), while an RRX-conjugated Donkey anti-Rat secondary (1:100, #712–295-150, Jackson Immuno) was used for Ly6G. Nuclei were counterstained with NucBlue Live Cell Stain (#R37605, Invitrogen, Waltham, MA, USA). Imaging was performed with a VS120 Virtual Slide Microscope and processed with Olyvia software (Olympus, Waltham MA, USA). Visiopharm image analysis software v.6.7.9.2590 (Visiopharm, Horsholm, Denmark) was used for fluorescent image analyses in a semi-automated fashion as previously described,[17,18] and images were pseudo-colored (αSMA and pCREB co-staining) in Visiopharm to increase accessibility.

2.5 | Tendon gliding and biomechanical testing

To quantify functional outcomes, tendon gliding and biomechanics were performed as previously described.[17,19] Briefly, hindlimbs were harvested through the knee joint and skin was removed to the ankle. The FDL tendon was visualized and freed just proximal to the tarsal tunnel where it was secured between two pieces of tape with cyanoacrylate. The leg was then secured to a custom jig with a clip. Serial loading was performed using small weights ranging from 0 to 19 g in a standardized fashion. Digital images were captured, and the metatarsophalangeal (MTP) joint flexion angle was measured from images at each weight using ImageJ. The gliding resistance was computed using the change in MTP flexion angles over the range of incremental loads. Increased gliding resistance and decreased MTP flexion angles are indicative of increased adhesive scar formation and inferior function. Upon completion of gliding testing, the FDL tendon was fully released from the tarsal tunnel and the foot was disarticulated from the tibia at the ankle, and the tendon gauge length was then measured. The healing tendon was kept intact in the hind paw to assess the mechanical properties of the healing tissue, including any potential contribution from scar tissue. The tape securing the proximal end of the FDL tendon and the toes of the hind paw were secured within opposite custom grips on an Instron 8841 DynaMight™ axial servo-hydraulic testing system (Instron Corporation, Norwood, MA, USA). Samples were loaded at a rate of 30 mm/min until failure. Force-displacement curves were used to determine maximum load to failure and stiffness.

2.6 | Single cell RNA isolation and sequencing

FDL tendons ($n = 3$ each for Ogerin and vehicle groups) were harvested at POD 14, pooled, and processed for single cell isolation as previously described.[20] Briefly, tendons were digested in low glucose DMEM (#11885084, Gibco) containing Collagenase I (5 mg/mL; #LS004196, Worthington Biochemical, Lakewood, NJ, USA) and IV

(1 mg/mL; #LS004188, Worthington Biochemical) for approximately 1 h, filtered (70 μm and 50 μm), pelleted (500×*g* for 10 min at 4°C), and resuspended in 0.5% Bovine Serum Albumin (BSA, Fraction V, #10735078001, Roche, Basel, Switzerland) in dPBS to a concentration of 1200 cells/μL.

Libraries were prepared and sequenced at the UR Genomics Research Center, with 10,000 cells per sample loaded into a Chromium Controller (10X Genomics, Pleasanton, CA, USA) for single-cell capture. Libraries were prepared using the Chromium Single Cell 3′ Kit (#1000075, 10X Genomics). Libraries were sequenced using the S2 NovaSeq flow cell system (Illumina, San Diego, CA), with an average of 879 million reads per sample (~83,000 reads per cell). Reads were processed using Cell Ranger (V8.0.0, 10X Genomics) and aligned to the mouse reference genome (GRCm38/mm10).

All scRNAseq analysis was performed using RStudio (v2023.12.0+369). Datasets from each treatment group were processed individually using Seurat (v4.4).[21] Low quality cells (low feature numbers, or mitochondrial gene content >5%) were excluded, resulting in 5182 cells for Vehicle, and 5933 cells for Ogerin treated repairs. Read data for each sample was normalized (normalization. method = "LogNormalize", scale.factor = 10,000) and the top 2000 most variable features were identified (selection. method = "vst") for downstream analysis. Vehicle and Ogerin treated datasets were then integrated (*FingIntegrationAnchors*, dims = 1:20), scaled, and dimensionality reduced using *RunPCA*, followed by unsupervised clustering with *FindNeighbors* (dims = 1:20), and *FindClusters* function (resolution = 0.25). Clusters were visualized as UMAP projections, and differentially expressed genes (DEGs) for each cluster were identified using *FindAllMarkers* (min.pct = 0.25, logfc.threshold = 0.25). To better understand how Ogerin treatment altered the gene expression profile within specific clusters, relative to vehicle treatment, gene ontology (GO) enrichment analysis was performed using DAVID Gene Functional Classification Tool (http://david.abcc.ncifcrf. gov; version 2023q4)[22,23] using the top 100 positively differentially expressed genes in specific clusters (tenocytes, epitenon cells, bridging cells, and resident macrophages) in Ogerin treated tendons.

To examine changes in predicted cell–cell communication, we utilized CellChat (v2.0).[24] CellChat objects were created for both Vehicle and Ogerin treated samples, and these objects were merged using *mergeCellChat*. The CellChatDB.mouse was used. The number and weight of interactions within each group were compared using *compareInteractions* (measure = "count", and measure = "weight", respectively). To define the differential number of interactions and interaction strength between different cell populations, *getMaxWeight* (attribute = "count", and attribute = "weight") was used. To identify changes in information flow between treatment groups, the *rankNet* function (mode = "comparison", do. stat = TRUE) was used. To identify differentially expressed genes between datasets, *identifyOverExpressedGenes* was used, with Ogerin set as the positive dataset (thresh.pc = 0.1, thresh.fc = 0.05, thresh.*p* = 0.05), followed by *netMappingDEG, subsetCommunication*, *extractGeneSubsetFromPair*. Data were plotted using *netVisual_bubble*, *netVisual_chord_gene*, *netVisual_circle*, and *netVisual_heatmap*.

2.7 | Statistical analysis

GraphPad Prism (GraphPad Software, San Diego, CA, USA) was used for statistical analyses. Normality was assessed using the Shapiro–Wilk normality test. GraphPad Prism was used to detect statistical outlier data points (ROUT method, *Q* value = 1%), though no outliers were detected and no data points were excluded. A student's *t*-test was performed for all quantitative analyses. Results are presented as means ± standard deviation. $p < 0.05$ was considered significant.

3 | RESULTS

3.1 | Ogerin modulates tendon fibroblast ↔ myofibroblast dynamics in vitro

To confirm that Ogerin could modulate tendon fibroblast ↔ myofibroblast dynamics in vitro in the same manner as lung, dermal, and intestinal fibroblasts,[14] primary tendon cells were isolated. We first assessed the effects of Ogerin on TGF-β-mediated myofibroblast differentiation. As expected, TGF-β treatment resulted in a significant increase in myofibroblast differentiation (as measured by the percentage of cells with αSMA+ stress fibers) ($p < 0.0001$, vs. vehicle control). However, co-treatment with Ogerin reduced differentiation in a dose-dependent manner (Figure 1A,B), such that myofibroblast differentiation in cells treated with TGF-β and 100 μM or 150 μM Ogerin was not significantly different from vehicle control cells that demonstrated very minimal differentiation. While cells treated with 50 μM Ogerin demonstrated a reduction in myofibroblast differentiation relative to TGF-β treated cells, differentiation was still elevated relative to vehicle controls ($p = 0.0148$). We then tested the ability of Ogerin to promote myofibroblast → fibroblast reversion. Following 24 h of TGF-β induced myofibroblast differentiation,
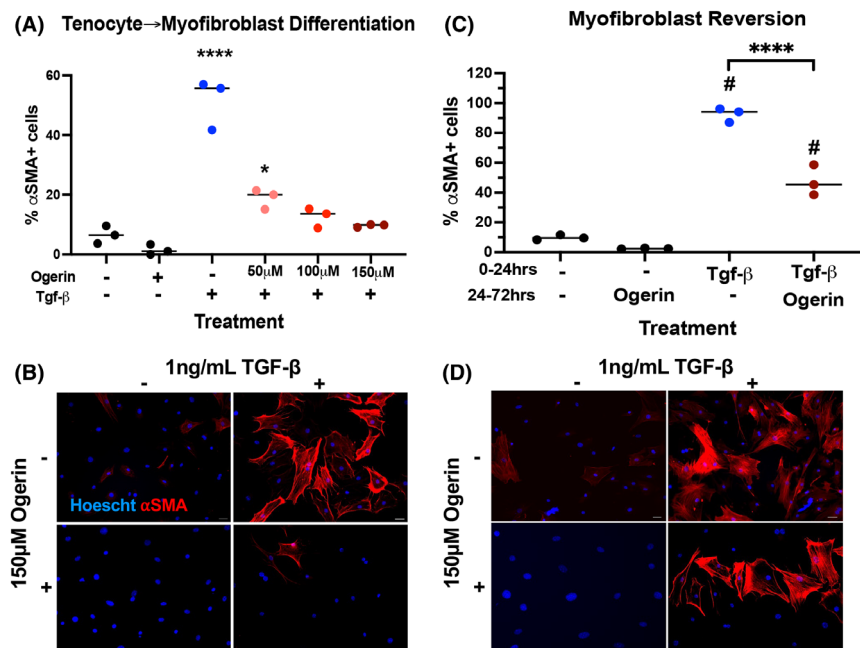
FIGURE 1 (A, B) Primary tendon cells were treated with vehicle controls, TGF-β and/or Ogerin (50-150 μM) for 24 h and myofibroblast differentiation was assessed via quantification of cells with αSMA+ stress fibers as a fraction of total cell number (Hoescht nuclei). (****) indicates $p < 0.0001$, and (*) indicates $p < 0.05$ vs. vehicle controls. (C, D) Primary tendon cells were treated with vehicle or 1 ng/mL TGF-β for 24 h followed by treatment with 150 μM Ogerin or vehicle for an additional 48 h, and the ability of Ogerin to induce myofibroblast → fibroblast reversion was assessed via quantification of the percent of cells with αSMA+ stress fibers. (#) indicates $p < 0.05$ versus vehicle controls, and (****) indicates $p < 0.0001$ between Tgf-β treated cells and cells treated with Tgf-β and Ogerin. Scale bars represent 100 μm.

Ogerin treatment (150 μM) significantly decreased the proportion of αSMA+ cells (50% reduction, $p < 0.0001$ vs. TGF-β treatment) (Figure 1C,D). Collectively, these data support Ogerin's ability to both blunt myofibroblast differentiation and promote myofibroblast reversion of tendon fibroblasts in vitro.

3.2 | Ogerin activates the Gpr68 Gαs pathway in vivo with treatment from day 8–12 post-surgery

Based on the promising in vitro ability of Ogerin to modulate tenocyte ↔ myofibroblast dynamics, we next assessed the impact of Ogerin on cell dynamics and tendon healing capacity in vivo. In the first arm of the study, we treated with Ogerin from POD 8–12, with the goal of blunting initial tenocyte → myofibroblast differentiation events (Figure 2A).[8] To confirm activation of GPR68 signaling via Ogerin treatment, we looked for activation of CREB signaling, via the presence of phospho-CREB (Ser133)+ cells as GPR68 activation induces cAMP/PKA/CREB signaling.[25] There was a significant increase in the percentage of pCREB+ cells in the Ogerin treated mice compared to the vehicle group (+22%, $p = 0.012$) (Figure 2B,C), indicating Ogerin-induced activation of GPR68 signaling.

In contrast to in vitro data, no difference in αSMA+ myofibroblast content was observed between Ogerin and vehicle-treated repairs at POD 14 ($p = 0.89$) (Figure 3A,B). Similarly, no apparent differences were observed histologically between Ogerin and vehicle-treated tendons with Alcian Blue/Hematoxylin/Orange G (ABHOG) stain (Figure 3C), and an initial provisional matrix was identified via Masson's Trichrome staining in both Ogerin and vehicle-treated mice (Figure 3D). We then examined pCREB expression in αSMA+ myofibroblasts and found strong pCREB activation in myofibroblasts in both vehicle-and Ogerin-treated tendons (yellow arrows, Figure S1), there were also αSMA+ myofibroblasts that did not express pCREB (orange arrows, Figure S1), and pCREB+ cells within the bridging tissue that were not αSMA+ (green arrows, Figure S1), highlighting the diversity of cells that activate pCREB during healing. No differences in F4/80+ macrophage content were observed between treatment groups (Figure S2).

We then assessed the impact of Ogerin treatment on functional and mechanical properties at POD 14. Ogerin treatment resulted in a significant increase in the maximum load to failure of the tendon (60% increase, $p = 0.036$), relative to vehicle treated repairs (Figure 4A). No differences in stiffness, MTP flexion angle, or gliding resistance (Figure 4B–D) were observed between Ogerin and Vehicle treated repairs at POD14.
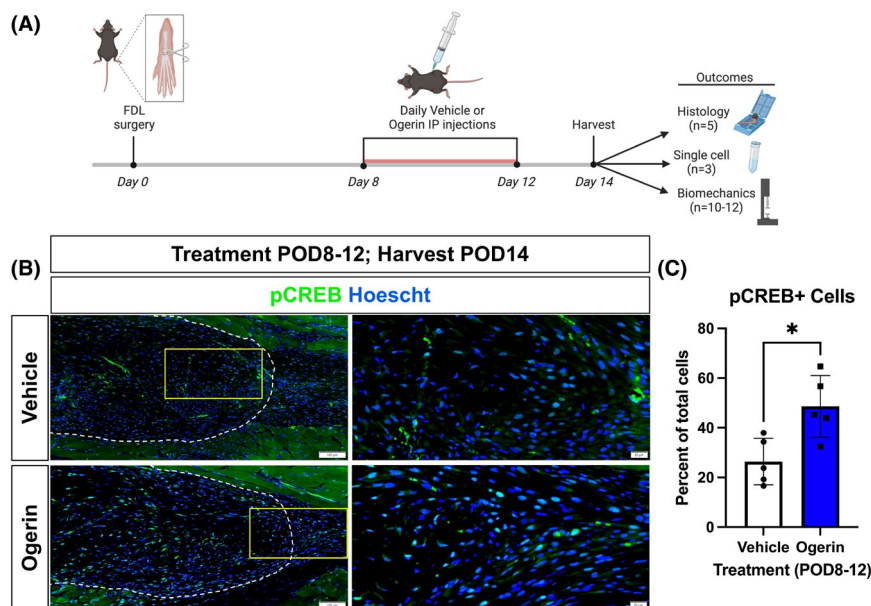
FIGURE 2 (A) Outline of experimental design for Ogerin treatment from post-operative day (POD) 8–12 (fibroblastic/proliferative phase of healing). (B) Assessment of Ogerin mediated Gpr68 activation of downstream signaling via pCREB (green). Nuclei are counterstained blue with Hoechst. Native tendon stubs are outlined in white, and the yellow boxes indicates location of higher magnification images. (C) Quantification of the percent pCREB+ cells, normalized to total nuclei. $N = 5$ per group. Student's t test was used to assess statistical significance. *$p \leq 0.05$. Scale bars $= 100\,\mu m$ in low power images, and $20\,\mu m$ in high power images.

3.3 | Ogerin treatment promotes ECM remodeling and alters cell communication patterns

Given the significant increase in tendon mechanics without a concomitant impact on the myofibroblast environment, we conducted single cell RNA sequencing (scRNASeq) to begin to define the effects of Ogerin treatment (POD8-12) on the cell environment at POD14. Unsupervised clustering resulted in 14 distinct cell clusters (Figure 5A) including cells from the epitenon (*Ccn3+*, *Pi16+*, *Col14a1+*, *Dpt+*), tenocytes (*Scx+*, *Tnmd+*, *Mkx+*), and a population associated with the bridging tissue at the healing site (*Tnn+*, *Comp+*, *Postn+*), which was defined in part via cross-referencing with our comprehensive scRNASeq dataset over the course of healing in this model.[20] In addition, two "injury-associated" cell clusters were identified based on their absence from scSeq of uninjured flexor tendons,[20] with one of these populations annotated as proliferating fibroblasts (*Mki67+*, *Cdc20+*, *Scx+*). Immune cell clusters including neutrophils (*S100a8+*, *S100a9+*, *Fpr1+*), T cells (*Cd3g+*, *Itk+*), and antigen presenting cells (*Ccr7+*, *H2-DMb2+*, *Cd209a+*) were also identified. In addition, two macrophage populations were identified: proliferating, injury-associated macrophages (*Mki67+*, *Adgre1+*, *Cd68+*, *Csf1r+*), and tendon-resident macrophages (*Adgre1+*, *Cd68+*, *Csf1r+*), with

this annotation based on tracking of macrophages from uninjured tendons in an integrated dataset that included uninjured and healing tendons.[20]

All populations were present in both vehicle and Ogerin treated samples (Figure S3A), and the proportion of each population was approximately equal between vehicle and Ogerin treated, except for neutrophils, which had a 2-fold increase in Ogerin versus vehicle treated repairs (Table S1), although no difference in the Ly6G+ area was observed by immunostaining between groups (Figure S4). While not an indicator of receptor protein expression levels, *Gpr68* was primarily expressed in resident macrophages and proliferating macrophages (Figure S3B). We then examined changes in gene expression within each cluster between Ogerin and vehicle treated repairs. Tenocytes (Figure 5B), epitenon cells (Figure 5C), and bridging cells (Figure 5D) demonstrated a consistent up-regulation in chemokine ligand genes (e.g., *Cxcl2*, *Ccl2*, *Ccl7*) and matrix metalloproteinases (MMPs) (e.g., *Mmp3*, *Mmp13*).

Gene ontology analysis demonstrated a consistent enrichment for biological processes associated with inflammatory response (GO: 0006954), chemokine mediated signaling (GO: 0070098), negative regulation of cell population proliferation (GO: 0008285), and neutrophil chemotaxis (GO: 0030593) in Ogerin treated repairs, relative to vehicle. An increase in extracellular matrix organization (GO: 0030198) was also observed in bridging cells of Ogerin treated tendons (Figure 5E–G). Resident

FIGURE 3 The impact of Ogerin treatment from post-operative day (POD) 8–12 on (A, B) αSMA+ myofibroblast differentiation (red staining). Scale bars represent 100 μm in low power images and 50 μm in high power images; (C) tissue morphology via Alcian Blue Hematoxylin Orange G (ABHOG) staining, and (D) Collagen presence via Masson's Trichrome staining at POD14. Scale bars represent 200 μm in low power images and 100 μm in high power images in (C, D). Native tendon stubs are outlined in white (A), black (C, D), and bridging tissue is outlined in red (C), and yellow (D). Boxes indicate location of higher magnification images. $N = 5$ per group. Student's t-test was used to assess statistical significance. (*) indicates $p \leq 0.05$.
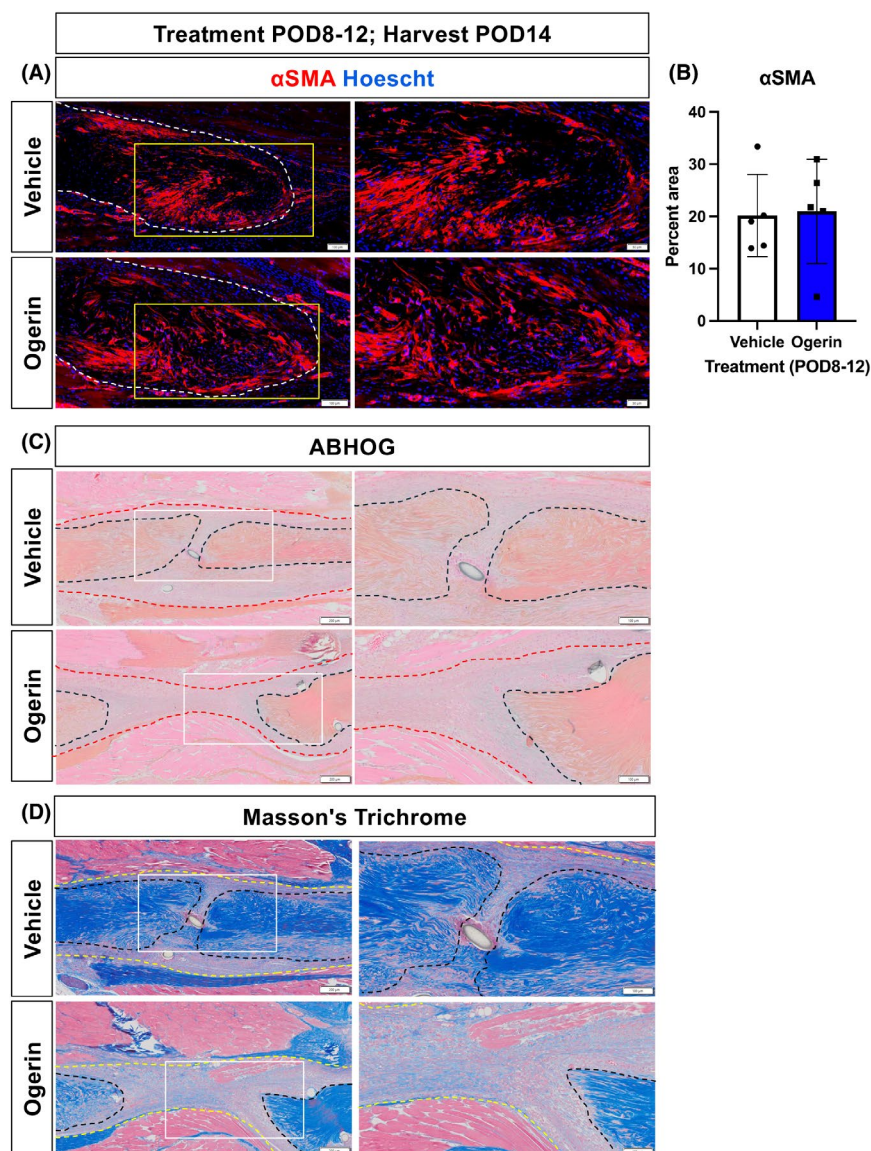
macrophages in Ogerin treated tendons had upregulated expression of ECM genes including *Col3a1* and *Postn* (Figure 5H) with enrichment in biological processes associated with inflammatory response (GO: 0006954), extracellular matrix organization (GO: 0030198), and negative regulation of cell population proliferation (GO: 0008285) (Figure 5I). Minimal differential gene expression was observed in all other populations between Ogerin and vehicle-treated samples (Figure S1C). To determine if Ogerin had any impact on the proliferation status of different cell populations, we examined expression of *Mki67*, *Pcna*, and *Mcm6*. No differences in *Mki67* expression were observed between vehicle and Ogerin treated groups, with resident macrophages, proliferating fibroblasts, and proliferating injury associated macrophages being the main *Mki67* expressing populations in both groups (Figure S5A). While *Pcna* was more broadly expressed across populations, no striking differences were seen as a

function of Ogerin treatment (Figure S5B). Finally, *Mcm6* was primarily expressed in proliferating injury associated macrophages, though no differences were seen between vehicle and Ogerin treatment; however, there was an increase in *Mcm6* expression in Ogerin treated T cells, relative to vehicle (Figure S5C).

Based on these data we then proceeded with subsequent analysis of the predicted communication patterns within and between cell populations using CellChat. Similar numbers of inferred interactions (15,153 for vehicle, 15,248 for Ogerin) (Figure S6A) and interaction strength (vehicle: 441; Ogerin: 435) (Figure S6B) were observed between groups. We then looked at interaction number and strength by cell cluster (red shades indicate increased signaling in Ogerin versus vehicle, and blue shades indicate decreased signaling in Ogerin vs. vehicle, Figure 6A). There was a substantial decrease in interaction number in Ogerin treated tendons both within the proliferating
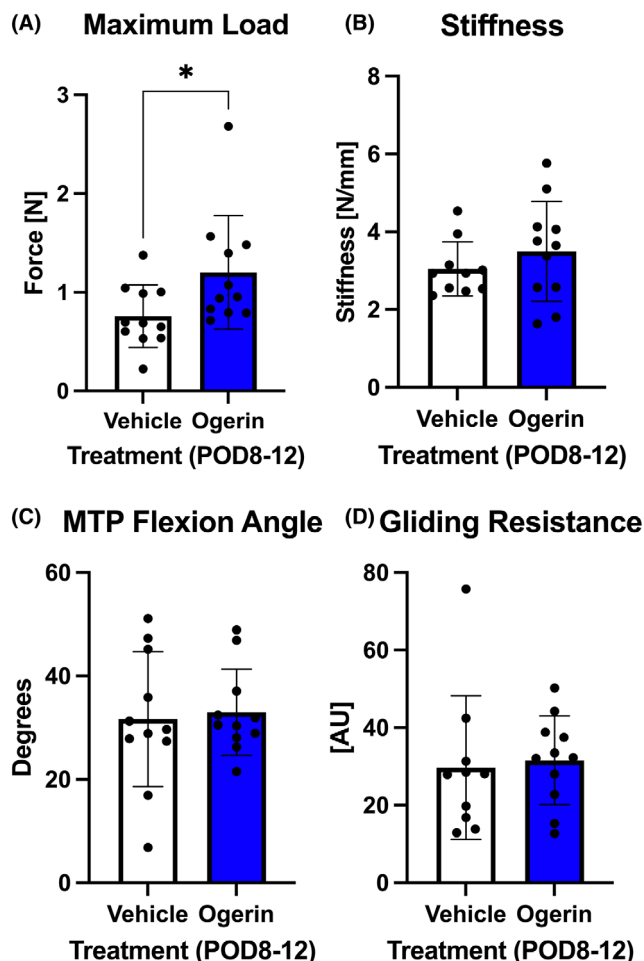
(A) Maximum Load

(B) Stiffness

(C) MTP Flexion Angle

(D) Gliding Resistance

FIGURE 4 Assessment of (A) maximum load at failure, (B) stiffness, (C) metatarsophalangeal (MTP) joint range of motion, and (D) gliding resistance from mice treated with Ogerin or vehicle from post-operative day (POD) 8–12, with tendons harvested at POD 14. $N = 10$–12 per group. Student's t-test was used to assess statistical significance. (*) indicates $p \leq 0.05$.

fibroblast cluster itself, and from other "fibroblast" populations (i.e., epitenon, tenocytes, and bridging cells) to proliferating fibroblasts. Moreover, there was a decrease in signaling strength in Ogerin treated tendons from fibroblast populations (i.e., epitenon, tenocytes, bridging cells, proliferating fibroblasts) to recruited immune cells (i.e., proliferating macrophages, APCs, T cells). However, there was also an increase in interaction number and interaction strength to neutrophils from nearly all other populations in Ogerin treated tendons (Figure 6A).

We first examined the specific signaling pathways that were shifted as a function of Ogerin treatment. More than 25 signaling pathways were putatively upregulated in Ogerin-treated tendons, including CXCL, CCL, NRG (Neuregulin), and CHAD signaling pathways (Figure 6B). Based on the increased expression of CXCLs and CCLs genes in Ogerin-treated tenocytes, epitenon cells, and bridging cells, we further interrogated Ogerin-driven

changes in CCL and CXCL signaling. While modest differences in CCL signaling were observed with Ogerin treatment across different populations (Figure S6C,D), CXCL signaling was substantially increased from all populations, particularly resident macrophages and epitenon cells to neutrophils (Figure 6C), perhaps explaining the >2-fold increase in neutrophil content in Ogerin-treated tendons. Moreover, there was a predicted increase in Cxcr2-related signaling in Ogerin-treated neutrophils (Figure S7), further supporting increased CXCL-CXCR2 signaling as a mechanism of increased neutrophil recruitment with Ogerin treatment.

We next examined changes in Collagen signaling due to its requirement in restoring functional integrity of the healing tendon. A heat map of Collagen signaling between populations (Figure 6D) indicates elevated Collagen signaling in epitenon, tenocytes, bridging cells, and proliferating fibroblasts with Ogerin treatment, relative to vehicle. Based on this, we then examined signaling changes from the epitenon, tenocytes, and bridging cells to the resident macrophage population. In Ogerin-treated repairs, there was a predicted upregulation in CD44, SDC4, and CD47 receptor communication in resident macrophages, though the primary ligands that were predicted to signal with these receptors varied by population, with COL1a1/COL1a2 ligands from epitenon cells, SPP1 and THBS4 ligands from tenocytes, and FN1 and THBS4 being the primary ligands from bridging cells (Figure S8A). Interestingly, the predicted ligand-receptor interactions between these populations were different in vehicle-treated tendons, with epitenon cells primarily signaling through FN1 from the epitenon, COL1a1 from tenocytes, and COL6a1/COL6a2 from the bridging cells to resident macs. Finally, we examined predicted signaling changes from resident macrophages to epitenon cells, tenocytes, and bridging cells. In Ogerin-treated tendons, SPP1 was the predominant resident macrophage ligand, with predicted communication with CD44 as the primary ligand on all three cell types, followed by ITGAV-ITGB1 in epitenon cells and tenocytes, and ITGA11-ITGB1 in bridging cells. In contrast, vehicle-treated tendons had ITGA4-ITGB1 to Vcam1 as the primary predicted upregulated signaling pathways from resident macrophages to epitenon cells, tenocytes, and bridging cells (Figure S8B).

3.4 | Ogerin treatment during tendon remodeling does not facilitate myofibroblast reversion or clearance

Based on the ability of Ogerin to promote myofibroblast reversion in vitro, we examined the impact of delayed Ogerin treatment (POD 24–28) on myofibroblast
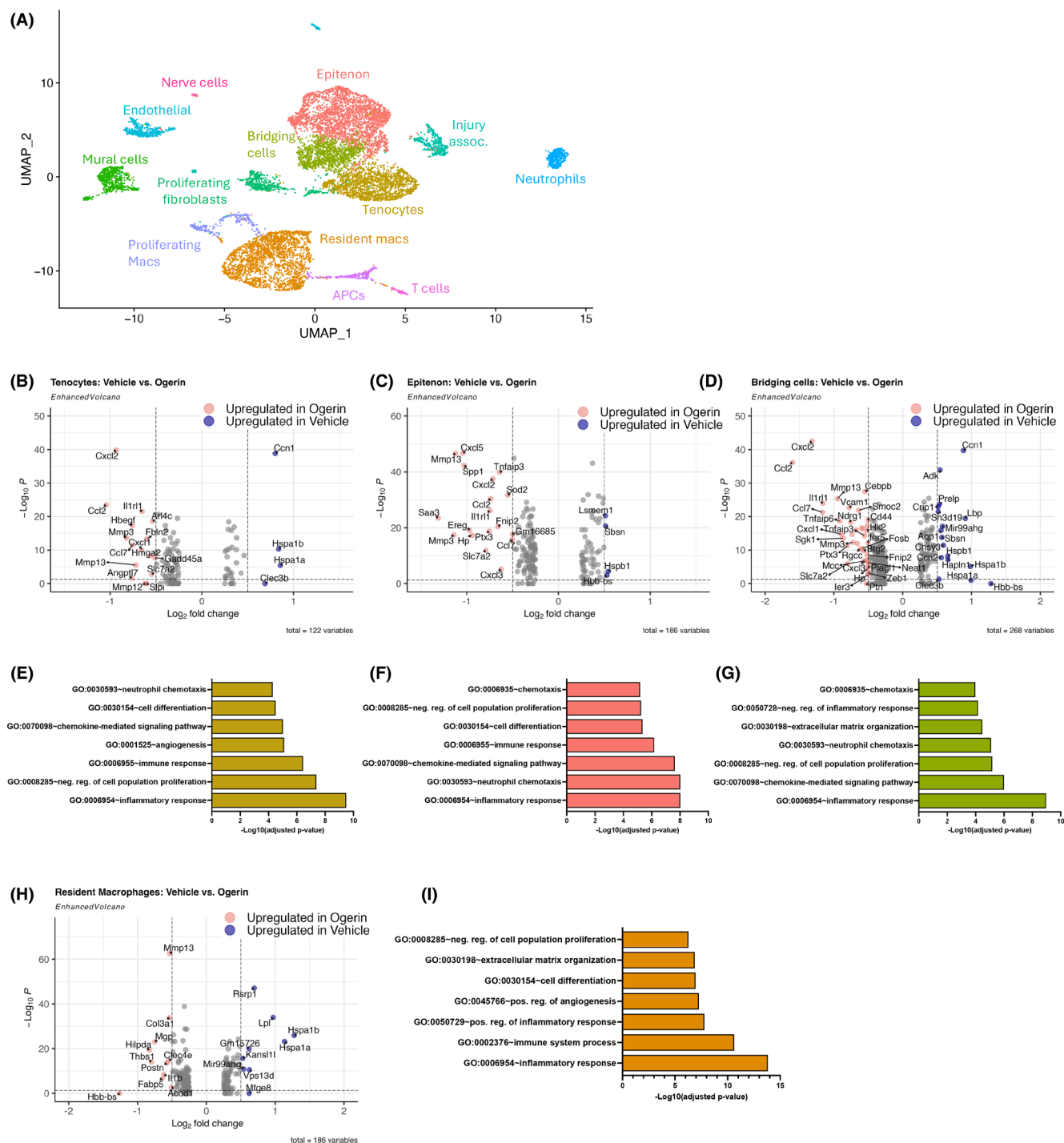
FIGURE 5 Single cell RNA sequencing of tendons treated with either Ogerin or vehicle from post-operative day 8–12 and harvested at day 14. (A) Unsupervised clustering and UMAP projection of cell clusters from integrated data from vehicle and Ogerin treated tendons. (B–D) Volcano plots of differentially expressed genes (DEGs) between Ogerin and vehicle treated tendons in (B) the tenocyte cluster, (C) the epitenon cell cluster, (D) the bridging cell cluster. (E–G) GO term biological processes based on top 100 upregulated DEGs in Ogerin treated tendons in (E) tenocytes, (F) epitenon cells, (G) bridging cells. (H) Volcano plot of DEGs in resident macrophages between Ogerin and vehicle treated tendons, (I) GO term biological processes upregulated in resident macrophages from Ogerin treated tendons.

persistence and morphological restoration during tendon healing (Figure 7A). Ogerin treatment was sufficient to induce a significant increase in CREB activation (19% increase in pCREB+ cells, $p < 0.05$), relative to vehicle treated repairs, supporting activation of GPR68 with this treatment regimen (Figure 7B,C). However, Ogerin treatment did not substantially alter the percent area of αSMA at the repair site between treatment groups
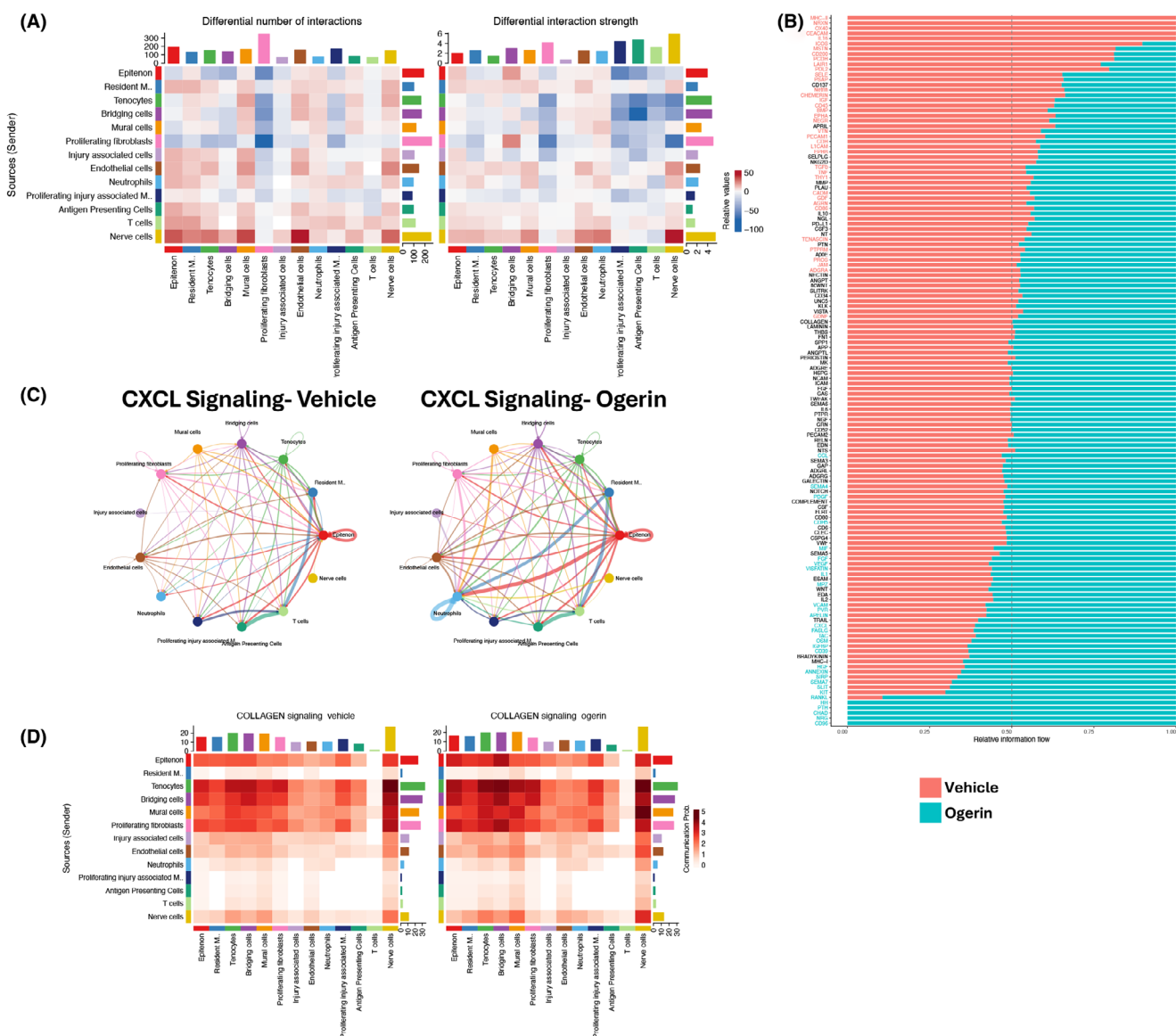
FIGURE 6 (A) Heatmap of the differential number (left) and interaction strength (right) between Ogerin and vehicle treated tendons. Red shades indicate relative increases in Ogerin treated, while blue shades indicate increases in vehicle treated repairs. (B) Predicted changes in signaling pathways between vehicle and Ogerin treated repairs. (C) Circle plot of CXCL signaling in vehicle and Ogerin treated tendons between cell clusters. (D) Heatmap of Collagen signaling by population in vehicle and Ogerin treated tendons.

(Figure 8A,B), suggesting that Ogerin treatment from POD 24–28 was insufficient to promote myofibroblast reversion or clearance in vivo. Moreover, the morphology of healing tendons was not markedly different between vehicle and Ogerin treated tendons (Figure 8C,D).

4 | DISCUSSION

There is a tremendous clinical burden associated with acute tendon injuries and their unsatisfactory outcomes after surgical repair. In particular, the tendency to heal via fibrotic scar rather than regeneration of the native tendon structure poses substantial challenges

including restricted range of motion, insufficient mechanical properties, and risk of repair rupture. Despite this burden, there are currently no biological or pharmacological therapies to improve the tendon healing process. Given that the balance between physiological healing and tissue fibrosis is tipped toward fibrosis by excessive and/or prolonged extracellular matrix deposition, modulating cellular dynamics to facilitate sufficient matrix deposition and remodeling followed by resolution of the healing process represents an important opportunity to positively impact tendon healing outcomes. As such, we utilized Ogerin, a small molecule positive allosteric modulator of GPR68, with the goal of modulating myofibroblast dynamics during
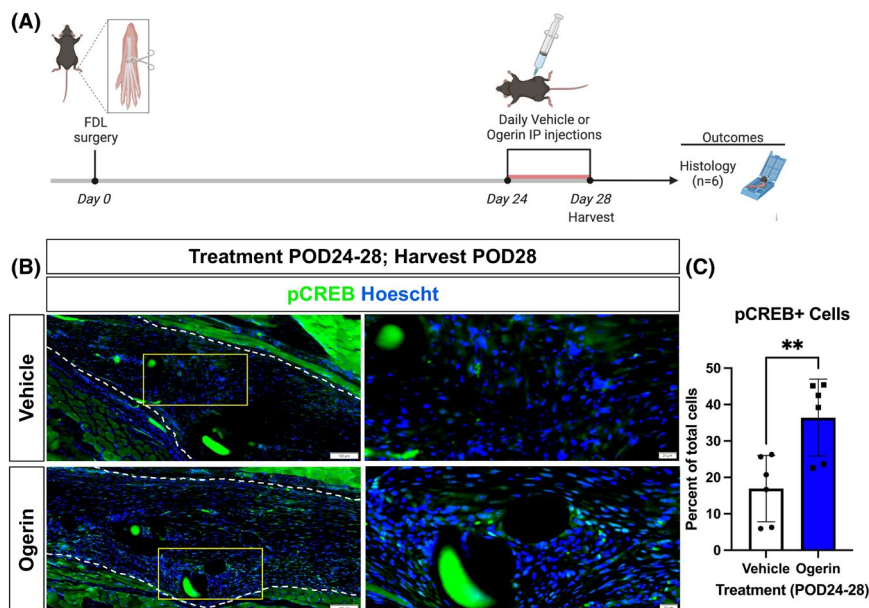
FIGURE 7 (A) Outline of experimental design for Ogerin treatment from post-operative day (POD) 24–28 (remodeling phase). (B) Assessment of Ogerin mediated GPR68 activation of downstream signaling via pCREB (green). Nuclei are counterstained blue with Hoechst. Tendons are outlined in white, and the yellow boxes indicates location of higher magnification images. (C) Quantification of the percent pCREB+ cells normalized to total nuclei. $N = 5$ per group. Student's t-test was used to assess statistical significance. $*p \leq 0.05$. Scale bars represent $100\,\mu m$ in low power images and $20\,\mu m$ in high power images.

healing, as Ogerin can blunt myofibroblast differentiation and promote reversion of mature myofibroblasts in multiple fibroblast populations.[14] Consistent with this, Ogerin successfully blunted TGF-β induced tenocyte → myofibroblast differentiation and promoted partial reversion of mature myofibroblasts to a basal tendon fibroblast state in vitro. Interestingly, the direct effects of Ogerin on fibroblast ↔ myofibroblast dynamics were not recapitulated in vivo, with no changes in αSMA+ myofibroblast content with either Ogerin treatment regimen, while Ogerin treatment from post-operative days 8–12 increased the max load at failure of the healing tendon, contrary to our hypothesis.

While the ability of Ogerin to modulate fibroblast ↔ myofibroblast states[14] was conserved in tendon cells in vitro, perhaps one of the most surprising findings of this study was the lack of effect on myofibroblast content during in vivo healing. Indeed, we initially hypothesized that Ogerin treatment from POD 8–12 would be detrimental to the healing process, given the likely role for myofibroblasts in the elaboration of the provisional collagen matrix.[8] However, recent work by Wu et al. demonstrated that activation of CREB-1 decreased adhesion formation and improved functional outcomes.[26] While it is not clear if CREB-1 activation altered myofibroblast fate or function, our data are consistent with improved healing in the context of CREB activation, although the multifaceted nature of CREB signaling requires further context-specific consideration of both the means of CREB activation

and the subsequent transcriptional activation profile. Moreover, while phospho-CREB is routinely used as a read-out of Gpr68 activation,[25] phospho-CREB can be activated by multiple pathways. However, there is currently no other means to assess GPR68 activation in vivo, as the powerful iGlow GPR68 reporter has only been validated in vitro.[27] As such, even though the specificity of Ogerin for GPR68 has been well documented,[25] we are unable to provide direct evidence of Gpr68 activation in vivo.

One alternative explanation for the beneficial effects of Ogerin treatment without the expected myofibroblast phenotype relates to the pH of the healing environment. GPR68, the receptor on which Ogerin acts, is a pH-sensitive G-protein coupled receptor, and potential differences in pH between in vitro culture and in vivo tendon healing environments may impact how GPR68 responds to Ogerin treatment. Finally, the in vitro system used here and in previous studies is primarily focused on tissue-resident fibroblasts, and the ability of Ogerin to act directly on these cells is clear. However, our single cell data demonstrate that macrophages are the primary *Gpr68+* population during healing. While transcript levels, particularly for receptors, are not necessarily a faithful readout of protein expression, these data suggest that Ogerin's primary effects may not occur directly on fibroblasts/myofibroblasts in the complex cellular environment of tendon healing, but rather may occur indirectly via macrophages, for example. Alternatively, it is possible that the predominant Gpr68+ populations change over the course of
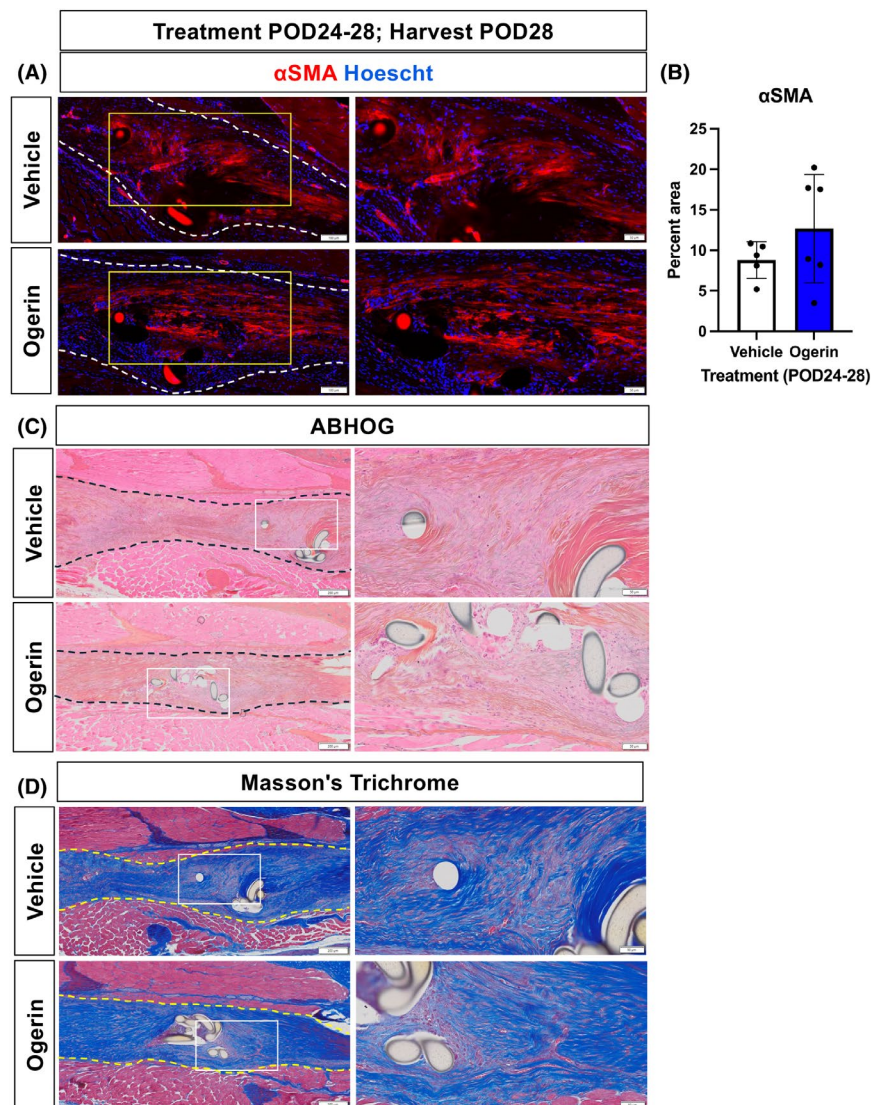
FIGURE 8 The impact of Ogerin treatment from post-operative day (POD) 24–28 on (A, B) αSMA+ myofibroblast differentiation (red staining), (C) tissue morphology via Alcian Blue Hematoxylin Orange G (ABHOG) staining, and (D) Collagen presence via Masson's Trichrome staining at POD 28. Tendon is outlined in white (A), black (C), and yellow (D). Boxes indicate location of higher magnification images. $N = 5–6$ per group. Student's t-test was used to assess statistical significance. (*) indicates $p \leq 0.05$. Scale bars represent 100 μm in low power images and 50 μm in high power images in (A). Scale bars represent 200 μm (low power) and 50 μm (high power) in (C, D).

healing and our treatment windows did not overlap with the in vivo periods of Gpr68 expression in fibroblasts/myofibroblasts.

With respect to the mechanisms underpinning increased max load at failure with Ogerin treatment from POD 8–12, single cell RNA sequencing provides some clues although additional work is needed as it is possible that analyzing the cell environment after treatment had concluded and at the time mechanical improvements had already been manifested resulted in us missing the most dynamic changes in the cell and transcriptional environment. Notably, the consistent increase in *Ccl2* and *Cxcl* expression in Ogerin treated tenocytes, epitenon cells, and bridging cells along with the enrichment in GO terms associated with 'inflammatory response' suggest that Ogerin may be promoting a more inflammatory environment. However, the decline in predicted communication from these cells to recruited immune cells (proliferating macrophages, APCs, T cells) and enrichment for GO terms associated with negative regulation of cell proliferation

suggest that Ogerin may actually be blunting the extrinsic immune response and the high level of cell proliferation that is typically observed during this phase of healing. Moreover, the elevated Mmp expression levels in the fibroblast populations and resident macrophages, as well as enrichment in biological processes associated with ECM remodeling in resident macrophages, and improved mechanical properties, suggest that Ogerin may be promoting resolution of the proliferative phase of healing and facilitating transition to earlier tissue remodeling. This is particularly important given that our mechanical testing paradigm keeps the healing tendon intact in the hind paw to account for any contribution of the scar tissue. As such, we were not able to determine if the mac load may be increased in part due to an increase in tissue cross-sectional area. However, increased expression of genes associated with ECM remodeling, suggests that the increase in max load may be the result of greater tissue integrity due to increased remodeling, though additional studies are needed to validate this.

With respect to limitations, we examined the effect of Ogerin treatment during two treatment windows intended to modulate myofibroblast dynamics during the fibroblastic/proliferative phase and during the remodeling phase. Given that Ogerin enhanced the healing process without a discernible impact on myofibroblast differentiation, it will be important to understand the effects of Ogerin treatment when administered at additional timepoints, different concentrations, or as local vs. systemic administration, as our ability to mechanistically interrogate the impact of Ogerin may be limited by the disconnect between the end of the treatment window and the timing of molecular analyses. Moreover, while Ogerin treatment from POD 8–12 increased tendon mechanics at POD 14, future studies are needed to understand whether these improvements are maintained long-term. Finally, only female mice were used in this study, as we have anecdotally observed a slight decrease in the rupture rate of repairs, possibly due to decreased fighting in group-housed female mice compared to male mice. Therefore, subsequent work will need to confirm that Ogerin-mediated improvements in healing are conserved in male mice, although we have not observed substantial sexual dimorphism during healing.

While additional work is needed to mechanistically define the functions of Ogerin in the context of tendon healing, these data support Ogerin's ability to modulate the cell environment and enhance healing, perhaps via altered cell signaling and communication patterns that promote earlier tissue remodeling and identify Ogerin as a novel therapeutic approach to improve tendon healing.

AUTHOR CONTRIBUTIONS

ACKNOWLEDGMENTS

CONFLICT OF INTEREST STATEMENT

DATA AVAILABILITY STATEMENT

ORCID

Andrew Rodenhouse https://orcid. org/0009-0007-8429-6281
Gilbert Smolyak https://orcid.org/0000-0001-9417-0884
Emmanuela Adjei-Sowah https://orcid. org/0000-0002-0219-043X
Neeta Adhikari https://orcid.org/0000-0003-2455-7682
Samantha Muscat https://orcid. org/0009-0009-9631-1383
Constantinos Ketonis https://orcid. org/0000-0003-4535-9079
Anne E. C. Nichols https://orcid. org/0000-0001-8754-7735
Robert M. Kottmann https://orcid. org/0000-0001-9316-6103
Alayna E. Loiselle https://orcid. org/0000-0002-7548-6653

REFERENCES

1. Klifto CS, Capo JT, Sapienza A, Yang SS, Paksima N. Flexor tendon injuries. *J Am Acad Orthop Surg*. 2018;26:e26-e35.
2. Mehrzad R, Mookerjee V, Schmidt S, Jehle CC, Kiwanuka E, Liu PY. The economic impact of flexor tendon lacerations of the hand in the United States. *Ann Plast Surg*. 2019;83:419-423.
3. Strickland JW. Development of flexor tendon surgery: twenty-five years of progress. *J Hand Surg Am*. 2000;25:214-235.
4. Strickland JW. Flexor tendon injuries: II. Operative technique. *J Am Acad Orthop Surg*. 1995;3:55.
5. Tang JB, Lalonde D, Harhaus L, Sadek AF, Moriya K, Pan ZJ. Flexor tendon repair: recent changes and current methods. *J Hand Surg Eur Vol*. 2022;47:31-39.
6. Dy CJ, Hernandez-Soria A, Ma Y, Roberts TR, Daluiski A. Complications after flexor tendon repair: a systematic review and meta-analysis. *J Hand Surg*. 2012;37:543-551.e541.
7. Best KT, Nichols AEC, Knapp E, et al. NF-κB activation persists into the remodeling phase of tendon healing and promotes myofibroblast survival. *Sci Signal*. 2020;13:eabb7209.
8. Ackerman JE, Best KT, Muscat SN, et al. Defining the spatial-molecular map of fibrotic tendon healing and the drivers of Scleraxis-lineage cell fate and function. *Cell Rep*. 2022;41:111706.
9. Pakshir P, Hinz B. The big five in fibrosis: macrophages, myofibroblasts, matrix, mechanics, and miscommunication. *Matrix Biol*. 2018;68-69:81-93.
10. Klingberg F, Hinz B, White ES. The myofibroblast matrix: implications for tissue repair and fibrosis. *J Pathol*. 2013;229:298-309.

11. Tomasek JJ, Gabbiani G, Hinz B, Chaponnier C, Brown RA. Myofibroblasts and mechano-regulation of connective tissue remodelling. *Nat Rev Mol Cell Biol*. 2002;3:349-363.

12. Huang AH, Lu HH, Schweitzer R. Molecular regulation of tendon cell fate during development. *J Orthop Res*. 2015;33:800-812.

13. Yu X, Huang X-P, Kenakin TP, et al. Design, synthesis, and characterization of Ogerin-based positive allosteric modulators for G protein-coupled receptor 68 (GPR68). *J Med Chem*. 2019;62:7557-7574.

14. Bell TJ, Nagel DJ, Woeller CF, Kottmann RM. Ogerin mediated inhibition of TGF-β(1) induced myofibroblast differentiation is potentiated by acidic pH. *PLoS One*. 2022;17:e0271608.

15. Nichols AEC, Muscat SN, Miller SE, Green LJ, Richards MS, Loiselle AE. Impact of isolation method on cellular activation and presence of specific tendon cell subpopulations during in vitro culture. *FASEB J*. 2021;35:e21733.

16. Ackerman JE, Loiselle AE. Murine flexor tendon injury and repair surgery. *J Vis Exp*. 2016;115:54433.

17. Muscat S, Nichols AEC, Gira E, Loiselle AE. CCR2 is expressed by tendon resident macrophage and T cells, while CCR2 deficiency impairs tendon healing via blunted involvement of tendon-resident and circulating monocytes/macrophages. *FASEB J*. 2022;36:e22607.

18. Ackerman JE, Nichols AE, Studentsova V, Best KT, Knapp E, Loiselle AE. Cell non-autonomous functions of S100a4 drive fibrotic tendon healing. *elife*. 2019;8:e45342.

19. Hasslund S, Jacobson JA, Dadali T, et al. Adhesions in a murine flexor tendon graft model: autograft versus allograft reconstruction. *J Orthop Res*. 2008;26:824-833.

20. Nichols AEC, Wagner NW, Ketonis C, Loiselle AE. Epitenon-derived cells comprise a distinct progenitor population that contributes to both tendon fibrosis and regeneration following acute injury. *bioRxiv*. 2023.

21. Hao Y, Hao S, Andersen-Nissen E, et al. Integrated analysis of multimodal single-cell data. *Cell*. 2021;184:3573-3587.e29.

22. Sherman BT, Hao M, Qiu J, et al. DAVID: a web server for functional enrichment analysis and functional annotation of gene lists (2021 update). *Nucleic Acids Res*. 2022;50:W216-W221.

23. Huang da W, Sherman BT, Lempicki RA. Systematic and integrative analysis of large gene lists using DAVID bioinformatics resources. *Nat Protoc*. 2009;4:44-57.

24. Jin S, Guerrero-Juarez CF, Zhang L, et al. Inference and analysis of cell-cell communication using CellChat. *Nat Commun*. 2021;12:1088.

25. Wiley SZ, Sriram K, Liang W, et al. GPR68, a proton-sensing GPCR, mediates interaction of cancer-associated fibroblasts and cancer cells. *FASEB J*. 2018;32:1170-1183.

26. Wu L-M, Wang Y-J, Li S-F, et al. Up-regulation of CREB-1 regulates tendon adhesion in the injury tendon healing through the CREB-1/TGF-β3 signaling pathway. *BMC Musculoskelet Disord*. 2023;24:325.

27. Ozkan AD, Gettas T, Sogata A, Phaychanpheng W, Zhou M, Lacroix JJ. Mechanical and chemical activation of GPR68 probed with a genetically encoded fluorescent reporter. *J Cell Sci*. 2021;134:jcs255455.

SUPPORTING INFORMATION

Additional supporting information can be found online in the Supporting Information section at the end of this article.